Effective Elastic Coefficients for Reinfoced Composite Material – 17029

Cheo Kyung Lee*, Sothee Lun*, Sung Paal Yim **

* Handong Global University
3 Namsong-ri, Heunghae-eub, Buk-gu, Pohang, Kyungbuk, 791-708
Republic of Korea

** Korea Atomic Energy Research Institute
P.O. Box 150, Yusong, Daejon, 305-600
Republic of Korea

ABSTRACT

The effective elastic coefficients for heterogeneous media periodic on the microscale are calculated by solving the micro-cell elastostatic problem numerically. The cell problem is obtained by applying the homogenization theory to periodic composite media. The geometry has a small inclusion of circular cross-section with longitudinal and transverse ribs which is embedded in the background material. The deformation is caused by traction force distributed on the interface between the two regions of different elastic moduli. The displacements are calculated by using ABAQUS and are used to determine the effective elastic coefficients on the macroscale. The effects of the existence of reinforcement are with ribs are discussed.

INTRODUCTION

The structural strength is enhanced when small inclusions of higher strength are inserted. For example, concrete structures are enhanced by steel reinforcement bars placed in the region where tensile force is applied. For safe and reliable operation of underground nuclear waste repository it is essentially important to secure large enough elastic properties to ensure reliable functioning of the facility. Therefore it is essential to know the elastic characteristics of composite media based on theoretically sound approach.

A micro-cell geometry with inclusions of the shape of circular cross-section with longitudinal ribs at the top and bottom of the cross-section and transverse ribs that connect the longitudinal ones is considered. The inclusions are distributed periodically in space in the solid background medium.

The theoretical approach is based on the homogenization theory which systematically combines the processes on the microscale (of order l) and deduces the governing equations and the effective coefficients on the macroscale (of order L) [1]. It is assumed that the two spatial scales are disparate so that $l << L$. Under two basic assumptions, (i) the periodicity of the medium structure on the microscale with periodic length l and (ii) the periodicity of all variables and material properties with the same periodic length l. The periodicity assumption is not restrictive because the

distributions and arrangements over the periodic length are quite arbitrary and pretty much all conceivable distribution patterns are possible. Only the efforts to carry out the elastostatic analysis will be different depending on the complexity of the distribution inside the unit micro-cell.

The theoretical developments start from the basic governing laws on the microscale (the equilibrium equations and constitutive laws). With multiple-scale perturbation expansion the governing laws on the macroscale are deduced with no recourse to empirical or experimental assumptions. Throughout the process certain microscale boundary-value problems in a unit cell are defined whose solution is used in the calculation of the effective macroscale elastic coefficients. If the inclusion geometry is specified, the solution to the unit cell problem is usually found by numerical method. The software package ABAQUS is specifically used to solve the elastostatic boundary-value problems defined on the microscale.

It is shown that the effective macroscale elastic coefficients increase along the direction of apparently larger reinforcement size. It is also shown that the penetration length affects the elastic coefficients so that along the direction of full penetration of the reinforcement bar it becomes the maximum.

It is noted that the computational approach adopted in this study starts from the basic governing relations on the microscale without making empirical or phenomenological assumptions. Then the multiple-scale analysis is used to deduce the effective relations (governing equations and constitutive laws) on the microscale. Therefore, in principle, if the microscale geometrical characteristics and the material properties are known, the effective coefficients on the macroscale can be calculated.

THE GOVERNING RELATIONS ON THE MICROSCALE

The composite medium is assumed to be composed of a solid region($\Omega 1$) and another solid region($\Omega 2$) that fills the unit cell on the microscale. Each region is assumed to be connected throughout the composite medium. Solid deformation takes palce by macroscopically imposed strain over the medium.

The basic governing equations in the solid domains ($\Omega 1$ and $\Omega 2$) and the boundary conditions on the interface(Γ) are described which is given in the process of multiple-scale expansion.

In each region, the quasi-static equilibrium equation with Hooke's law must be satisfied.

On the boundary Γ between the two regions, the continuity of the displacement, and the continuity of stress must be satisfied.

In summary, the equilibrium equation and the Hooke's law are written as

$$\nabla \cdot {}^{[a]}\boldsymbol{\sigma} = \frac{\partial\, {}^{[a]}\sigma_{ij}(\mathbf{x})}{\partial x_j} = 0 \qquad \mathbf{x} \in \Omega_a \ (a = 1, 2) \tag{Eq. 1}$$

$${}^{[a]}\sigma_{ij} = C^{[a]}_{ijkl}\, {}^{[a]}e_{kl} \quad \mathbf{x} \in \Omega_a \ (a = 1, 2) \tag{Eq. 2}$$

where ${}^{[a]}\sigma_{ij}$ and ${}^{[a]}e_{kl}$ are the solid stress and strain in Ω_a and $C_{ijkl}^{[a]}$ is the elastic coefficient tensor of rank 4. Summation is assumed for repeated indices (summation convention).

The boundary conditions on Γ are

$$ {}^{[1]}v_i = {}^{[2]}v_i \quad \mathbf{x} \in \Gamma \qquad \text{(Eq. 3)} $$

$$ {}^{[1]}\sigma_{ij} n_j = {}^{[2]}\sigma_{ij} n_j \quad \mathbf{x} \in \Gamma \qquad \text{(Eq. 4)} $$

where n_j is the unit normal vector on Γ pointing from $\Omega 1$ to $\Omega 2$.

The governing equations and the boundary conditions are then normalized and the multiple-scale expansion is carried out.

MULTIPLE SCALE ANALYSIS

Recognizing the scale disparity in the process of elastic deformation, two distinct length scales are introduced: the microscale (the fast scale), which is equivalent to the representative elementary volume in the traditional sense, and the macroscale, the scale over which the processes of interest take place from the viewpoint of reservoir engineering and management.

The variables are expanded as perturbation series in the following small parameter

$$ \frac{\ell}{L} = \epsilon << 1 \qquad \text{(Eq. 5)} $$

in which ℓ is the microscale length and L is the macroscale length. Upon expansion of the governing equations and boundary conditions, the microscale boundary-value problems are investigated according to the respective order of ϵ and the effective macroscale governing equations and coefficients are derived.

In the process of the multiple scale analysis, two canonical micro-cell boundary-value problems are defined whose solutions are used in the calculation of the effective medium properties(effective macroscale coefficients) by averaging over the micro-cell volume[2].

THE MICRO-CELL BOUNDARY-VALUE PROBLEMS

If the solid displaement is expanded in a perturbation series,

$$ {}^{[a]}\mathbf{v} = {}^{[a]}\mathbf{v}^{(0)} + \epsilon\, {}^{[a]}\mathbf{v}^{(1)} + \epsilon^2\, {}^{[a]}\mathbf{v}^{(2)} + \cdots \quad \mathbf{x} \in \Omega_a \ (a = 1, 2) \qquad \text{(Eq. 6)} $$

The leading order term ${}^{[a]}\mathbf{v}^{(0)}$ is independent of the microscale and the correction terms are expressed as

$$ {}^{[a]}\mathbf{v}^{(1)} = {}^{[a]}\boldsymbol{\phi} : e'(\mathbf{v}^{(0)}) + \left\langle {}^{[a]}\mathbf{v}^{(1)} \right\rangle = {}^{[a]}\phi_i^{mn} e'_{mn}(\mathbf{v}^{(0)}) + \left\langle {}^{[a]}v_i^{(1)} \right\rangle \quad \mathbf{x} \in \Omega_a \ (a = 1, 2) \tag{Eq. 7} $$

where $\left\langle {}^{[a]}v_i^{(1)} \right\rangle$ is the unit-cell average of the left-hand side. The unit-cell average is defined as

$$ \langle f \rangle = \frac{1}{\Omega} \int_{\Omega} d\Omega \tag{Eq. 8} $$

The unknown functions ${}^{[a]}\boldsymbol{\phi} = {}^{[a]}\phi_i^{mn} \ (a = 1, 2)$ are the displacement in *i*-th direction due to macroscale unit strain $e'_{mn}(\mathbf{v}^{(0)})$ in Ω_a. They are the solutions of the following boundary-value problems:

$$ \nabla \cdot [\mathbf{C}^{[1]} : \mathbf{e}({}^{[1]}\boldsymbol{\phi})] + (\nabla \cdot \mathbf{C}^{[1]}) : \mathbf{II} = 0 \quad \mathbf{x} \in \Omega_1 \tag{Eq. 9a} $$

$$ \nabla \cdot [\mathbf{C}^{[2]} : \mathbf{e}({}^{[2]}\boldsymbol{\phi})] + (\nabla \cdot \mathbf{C}^{[2]}) : \mathbf{II} = 0 \quad \mathbf{x} \in \Omega_2 \tag{Eq. 9b} $$

$$ {}^{[1]}\boldsymbol{\phi} = {}^{[2]}\boldsymbol{\phi} \quad \mathbf{x} \in \Gamma \tag{Eq. 9c} $$

$$ \mathbf{C}^{[1]} : [\mathbf{II} + \mathbf{e}({}^{[1]}\boldsymbol{\phi})] \cdot \mathbf{n} = \mathbf{C}^{[2]} : [\mathbf{II} + \mathbf{e}({}^{[2]}\boldsymbol{\phi})] \cdot \mathbf{n} \quad \mathbf{x} \in \Gamma \tag{Eq. 9d} $$

$$ < {}^{[1]}\boldsymbol{\phi} > = < {}^{[2]}\boldsymbol{\phi} > = 0 \tag{Eq. 9e} $$

Equations (Eq. 9a and 9b) are the equilibrium equations in Ω_1 and Ω_2. Equations (Eq. 9c and 9d) are the continuity relations for the displacement and the traction on the interface. Equations (Eq. 9e) is imposed for the uniqueness of the solutions.

The effective elastic coefficients on the macrosclae are given as

$$ C'_{ijab} = \left\langle C^{[1]}_{ijab} \right\rangle + \left\langle {}^{[1]}\sigma_{ij}({}^{[1]}\boldsymbol{\phi}^{ab}) \right\rangle + \left\langle C^{[2]}_{ijab} \right\rangle + \left\langle {}^{[2]}\sigma_{ij}({}^{[2]}\boldsymbol{\phi}^{ab}) \right\rangle \tag{Eq. 10} $$

It is composed of two part : the volume weighted average of the elastic coefficients and the stress due to ${}^{[a]}\boldsymbol{\phi}$.

THE MICROCELL GEOMETRY, COMPUTATIONAL DOMAIN, AND MESH

The microcell geometry with sample meshes considered in this study is shown in Fig. 1 in which a half of the cross-section(Ω_1 and Ω_2) is shown in (a).

The region Ω_1 in the shape of circular cross-section with a small rectangular longitudinal rib at the top and a transverse rib connected to the longitudinal rib is shown in (b). The region Ω_2 is shown in (c). The front view of (b) and (c) combined is the same as that in (a).

The cell shown in Fig. 1(a) has dimensionless size of unity in the horizontal direction and 0.5 in the vertical direction. The radius of the circular cross-section is chosen to be 0.1.

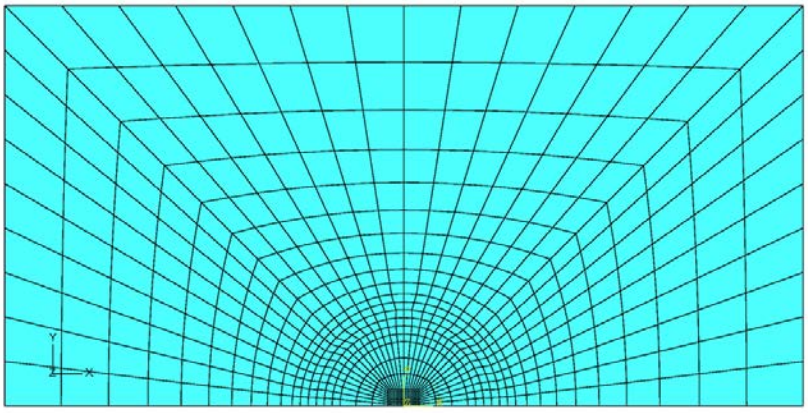

(a) Ω_1 and Ω_2

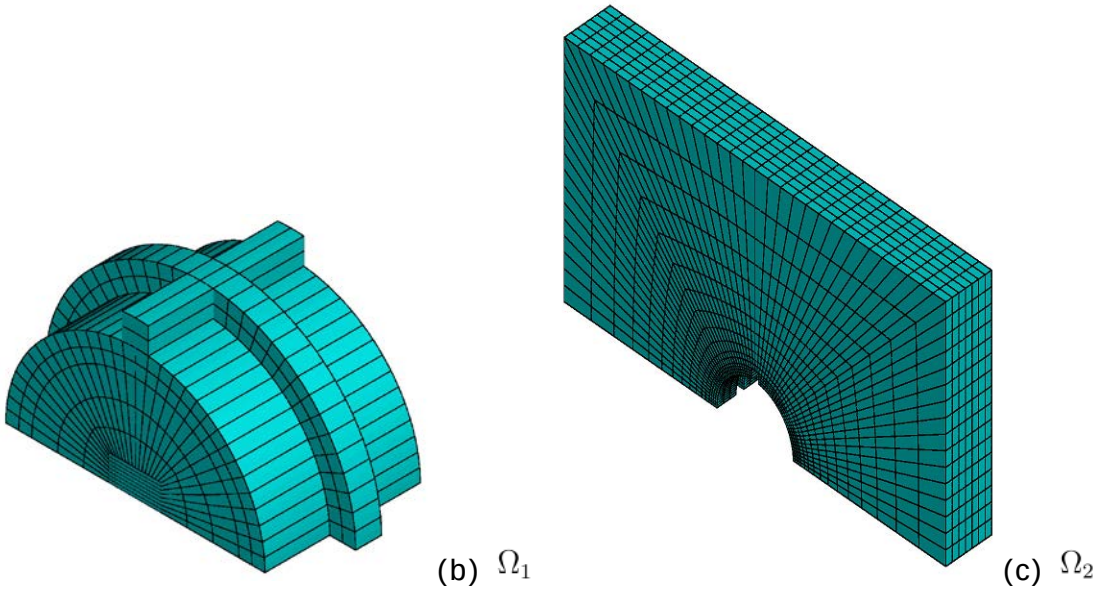

(b) Ω_1 (c) Ω_2

Fig.1 The microcell geometry: (a) Front view of a half of the cross-section, (b) Ω_1 in the shape of circular cross-section with longitudinal and transverse ribs, and (c) Ω_2.

Four progressively finer meshes are used and, for convenience, the three meshes for Ω_1 are shown in Fig. 2 (a)-(c).

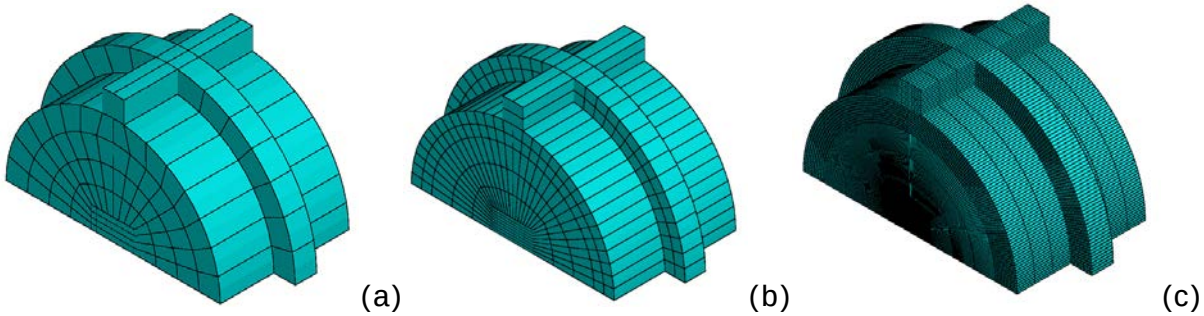

(a) (b) (c)

Fig. 2. Three different meshes: (a) Coarse, (b) Medium, and (c) Fine.

PROPERTIES OF THE SOLID MATERIALS IN Ω_1 AND Ω_2.

The solid materials in Ω_1 and Ω_2 are assumed to be isotropic. The elastic coefficient tensor is then[3]

$$C^{[a]}_{ijk\ell} = \lambda^{[a]}\delta_{ij}\delta_{k\ell} + \mu^{[a]}(\delta_{ik}\delta_{j\ell} + \delta_{i\ell}\delta_{jk}), \quad \lambda^{[a]} = \frac{E^{[a]}\nu^{[a]}}{(1-\nu^{[a]})(1-2\nu^{[a]})}, \quad \mu^{[a]} = \frac{E^{[a]}}{2(1+2\nu^{[a]})}$$

$$(a = 1, 2) \qquad \text{(Eq. 11)}$$

where $\lambda^{[a]}$ and $\mu^{[a]}$ are the Lame constants in Ω_a and δ_{ij} is Kronecker delta.

They are normalized by $E^{[1]}$ as follows:

$$\lambda^{[1]*} = \frac{\lambda^{[1]}}{E^{[1]}}, \ \lambda^{[2]*} = \frac{\lambda^{[2]}}{E^{[1]}}, \ \mu^{[1]*} = \frac{\mu^{[1]}}{E^{[1]}}, \ \mu^{[2]*} = \frac{\mu^{[2]}}{E^{[1]}} \qquad \text{(Eq. 12)}$$

in which symbols with superscript * are dimensionless.

The physical values are chosen as follows:

$E^{[1]}$ =2.00x10^{11} Pa, $\nu^{[1]}$=0.3; $E^{[2]}$=2.49x10^{10} Pa, $\nu^{[2]}$=0.21 (Eq. 13)

They are typical of steel and concrete. Hence the micro-cell can be regarded as realization of concrete material enhanced by steel bars with ribs. The normalized elastic coefficients then become

$$C^{[1]}_{xxxx}{}^{*} = \lambda^{[1]*} + 2\mu^{[1]*} = 1.3461, \quad C^{[1]}_{xxyy}{}^{*} = \lambda^{[1]*} = 0.5769, \quad C^{[1]}_{xyxy}{}^{*} = 2\mu^{[1]*} = 0.7692$$

$$C^{[2]}_{xxxx}{}^{*} = \lambda^{[2]*} + 2\mu^{[2]*} = 0.14, \quad C^{[2]}_{xxyy}{}^{*} = \lambda^{[2]*} = 0.0372, \quad C^{[2]}_{xyxy}{}^{*} = 2\mu^{[2]*} = 0.1028 \qquad \text{(Eq. 14)}$$

$$C^{[a]}_{xxxx}{}^{*} = C^{[a]}_{yyyy}{}^{*} = C^{[a]}_{zzzz}{}^{*} \quad C^{[a]}_{xxyy}{}^{*} = C^{[a]}_{yyzz}{}^{*} = C^{[a]}_{zzxx}{}^{*} \quad C^{[a]}_{xyxy}{}^{*} = C^{[a]}_{yzyz}{}^{*} = C^{[a]}_{zxzx}{}^{*} \ (a = 1, 2)$$

NUMERICAL RESULTS AND DISCUSSION

In this study, the cases of *ab=xx, yy* in (Eq. 10) are discussed, i.e., the macroscale strains are axial one in the x-, y- and z-directions. Some typical numerical results obtained from the finest mesh are shown for the case ab=xx..

Macroscale strain in x-dir.: ab=xx

The displacements ϕ^{xx}_x, ϕ^{xx}_y and ϕ^{xx}_z are shown in Fig. 3 (a) , (b) and (c). The displacements are due to the traction force on the interface which points inwards from the outer region (Ω_2) to the inner region (Ω_1). Because of perodicity it zero on the left and right boundaries. Hence it is positive in the left half of the cell and negative in the right half of the cell respectively.

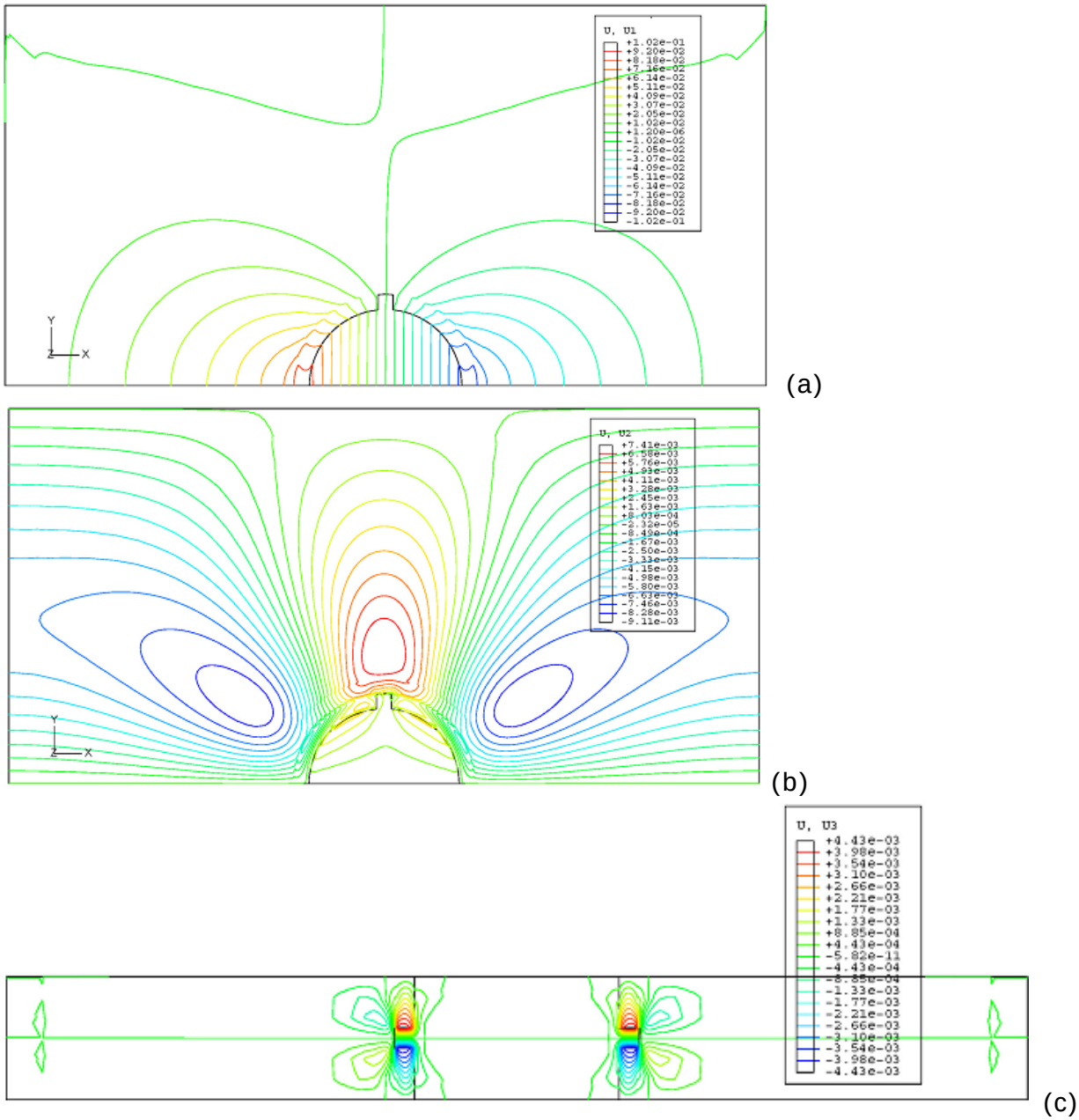

(a) (b) (c)

Fig. 3 The displacements ϕ_x^{xx}, ϕ_y^{xx} and ϕ_z^{xx}.

The normal strains $e_{xx}(\boldsymbol{\phi}^{xx})$, $e_{yy}(\boldsymbol{\phi}^{xx})$ and $e_{zz}(\boldsymbol{\phi}^{xx})$ are shown in Fig. 4 (a), (b), and (c). Because of the geometric symmetry about the center of the region the strains are symmetric about the center.

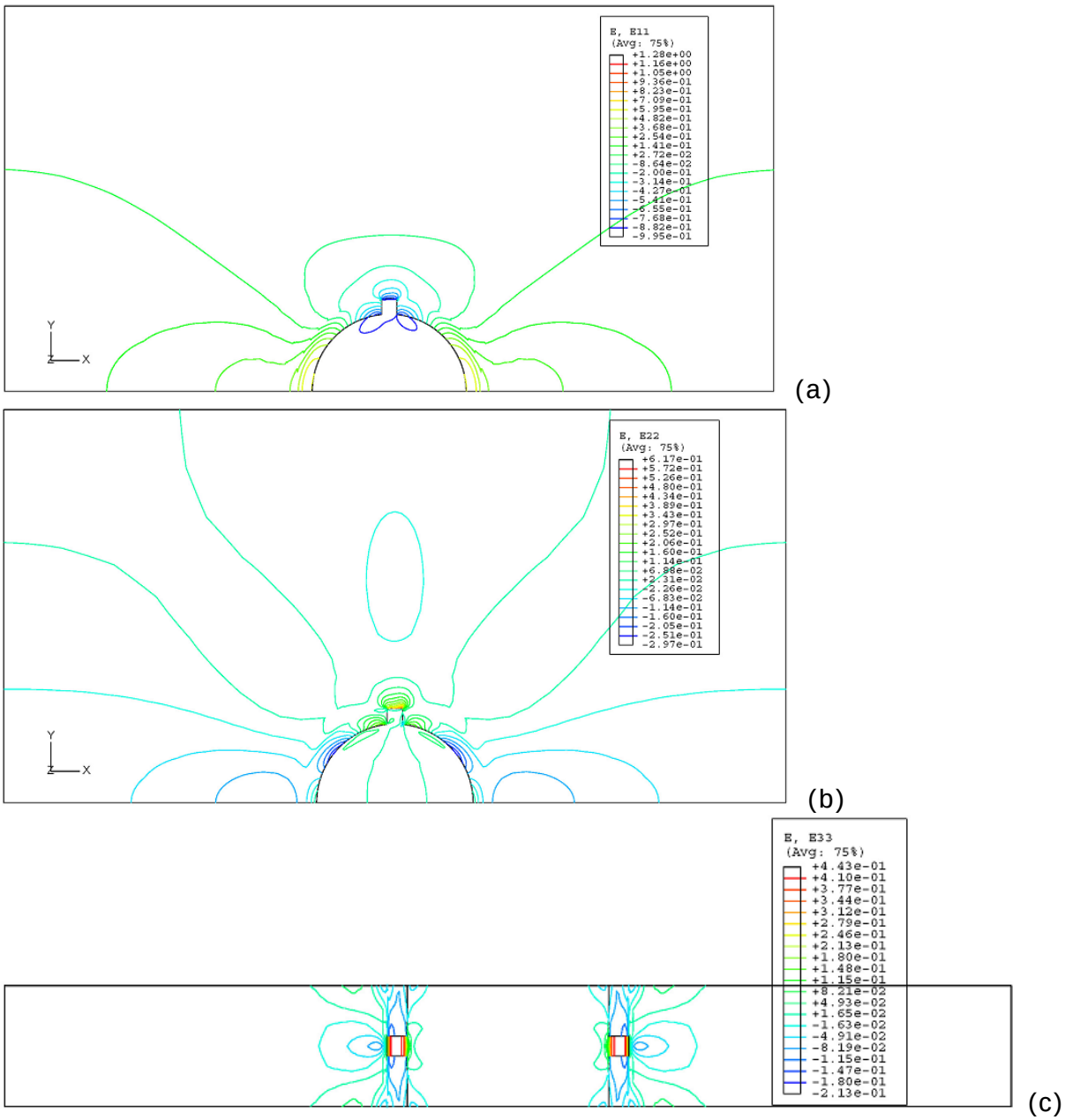

Fig. 4 The strains (a) $e_{xx}(\boldsymbol{\phi}^{xx})$, (b) $e_{yy}(\boldsymbol{\phi}^{xx})$ and (c) $e_{zz}(\boldsymbol{\phi}^{xx})$.

The stresses $\sigma_{xx}(\boldsymbol{\phi}^{xx})$, $\sigma_{yy}(\boldsymbol{\phi}^{xx})$ and $\sigma_{zz}(\boldsymbol{\phi}^{xx})$ are shown in Fig. 5(a) , (b) and (c). Due to the symmetry of the strains the stresses are symmetric about the center too.

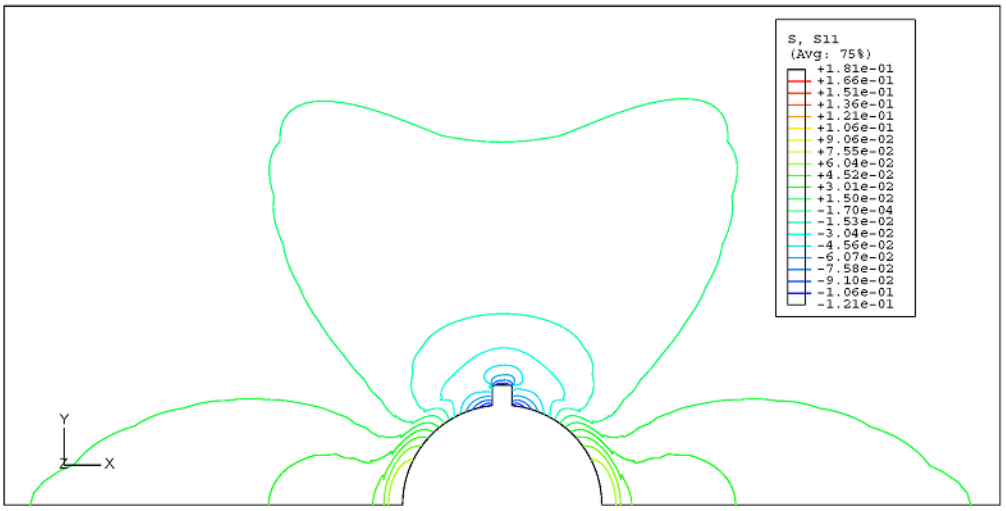

(a)

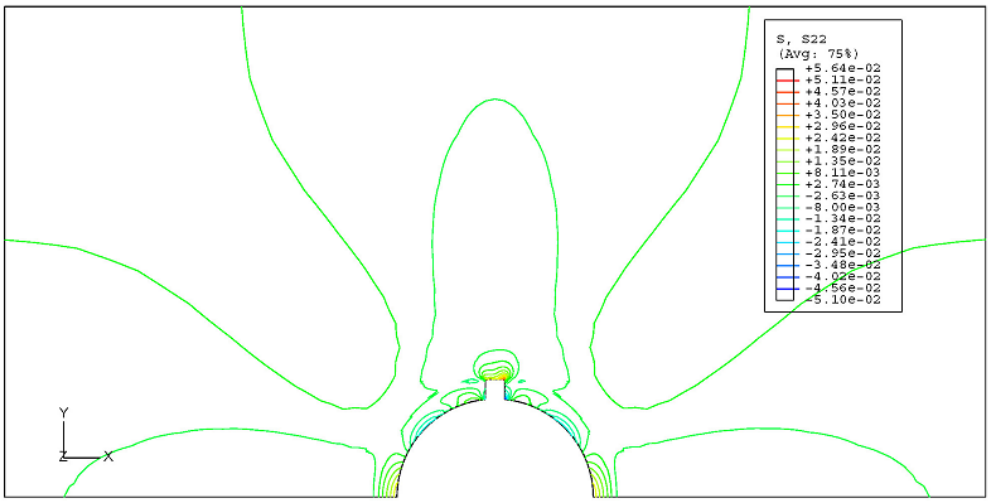

(b)

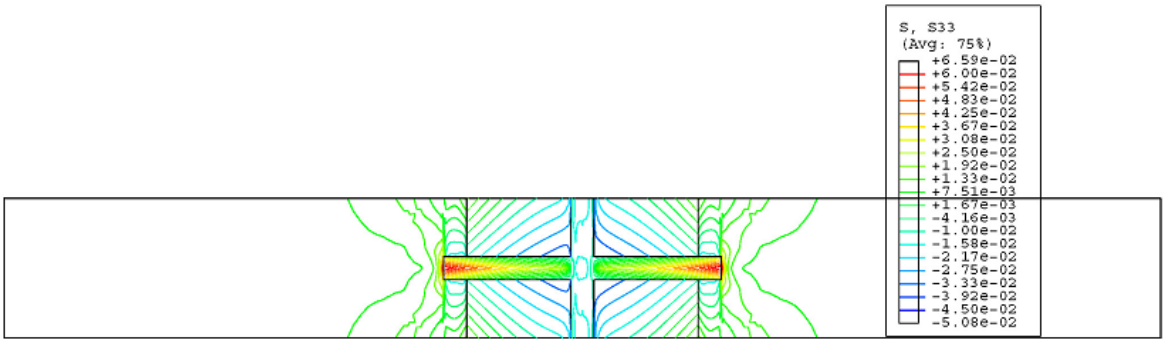

(c)

Fig. 5 stresses (a) $\sigma_{xx}(\boldsymbol{\phi}^{xx})$, (b) $\sigma_{yy}(\boldsymbol{\phi}^{xx})$ and (c) $\sigma_{zz}(\boldsymbol{\phi}^{xx})$.

THE EFFECTIVE ELASTIC COEFFICIENTS ON THE MACROSCALE

The volumes and their respective fractions are shown in Table 1.

Total vol. ($\Omega_1+\Omega_2$)=6.00E-02	Ω_1 = 2.06E-03	Ω_2 = 5.79E-02
Total fractional vol. = 1	f_1 = 3.43873E-02	f_2 = 9.65613E-01

Table 1 The volumes and their fractions.

From the calculations with the finest meshes in the previous section and (Eq. 10) and (Eq. 11), the effective elastic coefficients on the macroscale are summarized in Tables 2 to 4.

C'ijxx (ab=xx)

Mesh	ij=xx	ij=yy	ij=zz
Coarse	1.470748E-01	4.108857E-02	4.128230E-02
Medium	1.468771E-01	4.100090E-02	4.118391E-02
Fine	1.468470E-01	4.098962E-02	4.117049E-02
Finer	1.468152E-01	4.097840E-02	4.117295E-02

Table 2 The effective elastic coefficients on the macroscale (ab=xx).

C'ijyy (ab=yy)

Mesh	ij=xx	ij=yy	ij=zz
Coarse	3.963281E-02	1.510368E-01	4.203580E-02
Medium	3.953851E-02	1.508417E-01	4.193985E-02
Fine	3.952608E-02	1.508121E-01	4.192755E-02
Finer	3.951348E-02	1.507857E-01	4.193037E-02

Table 3 The effective elastic coefficients on the macroscale (ab=yy).

C'ijzz (ab=zz)

Mesh	ij=xx	ij=yy	ij=zz
Coarse	4.013919E-02	4.181405E-02	1.727569E-01
Medium	4.004893E-02	4.172665E-02	1.726968E-01
Fine	4.003574E-02	4.171399E-02	1.726888E-01
Finer	4.003036E-02	4.170903E-02	1.726882E-01

Table 4 The effective elastic coefficients on the macroscale (ab=zz).

It is seen the effective elastic coefficients converge quickly as the mesh become finer and finer and are satisfactorily accurate for the 'Finer' case.

The effective elastic coefficient C'yyyy (=1.507857E-01) is a little bit larger than C'xxxx (=1.468152E-01) because the extent of the reinforcement bar size is larger along y-direction due to the longitudinal ribs.

The effective elastic coefficient C'zzzz (=1.726882E-01) is somewhat larger than

C'yyyy (=1.507857E-01) since the reinforcement bar is fully penetrating along z-direction and also the transverse ribs add more rigidity along z-direction.

CONCLUSIONS

From the calculations of the effective elastic coefficients for a composite material with embedded reinforcement bars with longitudinal and transverse ribs the following conclusions are drawn.

1. The elastic coefficients obviously increase due to the existence of stronger reinforcement bars.
2. The elastic coefficient appears to be larger in the direction of apparently larger extent of the bar due to the longitudinal ribs.
3. The elastic coefficient is the largest along the direction of full penetration of the bar with enhancement due to the transverse ribs.

REFERENCES

1. C.K. LEE, "The Effective Elastic Coefficients of Porous Media with Simple Pore Geometries, Waste Management 14, Phoenix, AZ, USA.(2014).
2. C.K. LEE, M.Z. Htway, M.Z. and S. P. YIM, "Permeability and Dispersion Coefficients in Rocks with Fracture Network", Waste Management 14, Phoenix, AZ, USA. .(2014).
3. Y.C. FUNG, *Foundations of Solid Mechanics*, Prentice-Hall(1965).

ACKNOWLEDGEMENT

This research was supported by the National Research Foundation of Korea

(Grant: NRF-2010-0004808) funded by the Ministry of Education, Science and Technology. The financial support is gratefully acknowledged.